Journal of Power Sources 242 (2013) 478–485

Contents lists available at SciVerse ScienceDirect

Journal of Power Sources

journal homepage: www.elsevier.com/locate/jpowsour

Capacity fading mechanism in lithium sulfur cells using poly(ethylene glycol)-borate ester as plasticizer for polymer electrolytes

Zhaoqing Jin [a,*], Kai Xie [a], Xiaobin Hong [a], Zongqian Hu [b,**]

[a] Department of Material Science and Engineering, National University of Defence and Technology, Changsha 410073, China
[b] Beijing institute of Radiation Medicine, 27 Taiping Road, Beijing 100850, China

HIGHLIGHTS

- Anion receptor was used as plasticizer in gel polymer electrolyte for Li–S cell.
- Li–S cell with the gel polymer electrolyte shows an improvement in cycle performance.
- Anion receptor could inhibit the migration of polysulfide anions but not permanently.

ARTICLE INFO

Article history:
Received 1 April 2013
Received in revised form
8 May 2013
Accepted 20 May 2013
Available online 6 June 2013

Keywords:
Poly(ethylene glycol)-borate ester
Gel polymer electrolyte
Li–S cells
Capacity fading mechanism

ABSTRACT

Plasticizers of poly(ethylene glycol)-borate (PEG-B) esters are added into lithium-conducting gel polymer electrolyte (GPE) in Li–S cells in order to inhibit the unrestrained migration of polysulfide anions. An improvement of the electrochemical properties of the Li–S cell using GPE is observed upon addition of the plasticizers at room temperature. However, a slow decrease of discharge capacities follows after stable cycles. To understand the origin of the capacity fading, electrochemical impedance spectroscopies (EIS), scanning electron microscopy (SEM), X-ray Diffraction (XRD) and X-ray photoelectron spectra (XPS) are adopted. EIS measurements indicate that the decrease of capacity in the Li–S cell using GPE is related to the increase of interfacial resistance between GPE and anode. SEM studies combined with XRD and XPS measurements reveal the increase of interfacial resistance between GPE and anode is results from Li_2S corrosion products. Accordingly, the polysulfide anions precipitate on the anode surface, which leads to a reduction of the cycle life of the Li–S cell using GPE. Li-ion transference number measurement shows an increase of transference number before 20th cycles, and then decreased, which suggests that the GPE using PEG-B esters as plasticizers could inhibit the unrestrained migration of polysulfide anions at some time but not permanently.

1. Introduction

The Li–S cells represent a dramatic advance over lithium-ion cells in several respects. The most important is the specific energy (2600 Wh kg^{-1} in theoretical, 400–500 Wh kg^{-1} in practical), which is more than five times the energy of a Li-ion system [1]. This technology has been regarded as one of the candidates for next generation cell [2]. However, the main obstacle to realize Li–S cells is the bad cycle performance, which is mainly caused by the soluble intermediate lithium polysulfide (Li_2S_n, $3 \leq n \leq 8$) and the insoluble, highly insulative end productions (Li_2S_2 and/or Li_2S) [3–6]. Li_2S_2 and Li_2S produce a passivating layer deposited onto the surface of lithium electrode. This layer doesn't participate in the farther redox reaction of elemental sulfur anymore, and slows down or completely prevents further interaction of metal lithium with components of the electrolyte system, which contributes to the loss of active mass and the corrosion of electrodes, finally resulting in the decrease of coulombic efficiency of Li–S cells [7,8].

To improve the performance of Li–S cells, attentions have been paid to the sulfur cathode. Different kinds of carbon with special structure were used to prepare the S cathode with special structure, such as the highly ordered nanostructure cathode [9], the core–shell structure cathode [10], and the sandwich-type cathode [11], to reduce the dissolution of polysulfide anions from the cathode based on physical adsorption. However, these approaches are fundamentally ineffective, because the electric field and the concentration

* Corresponding author. Tel.: +86 731 84573149; fax: +86 731 84573150.
** Corresponding author.
E-mail addresses: jinzhaoqing1001@gmail.com (Z. Jin), huzongqian@gmail.com (Z. Hu).

0378-7753/$ – see front matter © 2013 Elsevier B.V. All rights reserved.
http://dx.doi.org/10.1016/j.jpowsour.2013.05.086

gradient between two electrodes will drive polysulfide anions to migrate toward Li anode.

Moreover, additives in liquid electrolyte have been studied as well. $LiNO_3$ had been regarded as an effective additive in liquid electrolyte, because the components of electrolyte with $LiNO_3$ react with lithium anode to form protective surface film. The film could prevent the reaction between lithium anode and polysulfides [12–14]. And other additives have also been studied, such as toluene [15], dimethyl methyl phosphonate [16], phosphorous pentasulfide [17]. However, the protective surface films formed by the additives are not so dense and stable that they couldn't prevent the parasitic reaction completely and continuously.

An alternative idea to improve the performance of Li–S cells is using the functional electrolyte to prevent the transporting of polysulfide anions, such as the single-ion polymer electrolyte [18], the room temperature ionic liquid [19,20], and the inorganic solid electrolytes [21,22]. These approaches prevent polysulfide anions contact with Li anode directly.

Recently, additions of anion receptors with Lewis acidity as plasticizer into the polymer electrolytes have been studied. The anion receptors with Lewis acidity are expected to interact with Lewis basic anions and trap them, which achieves high transference number for lithium ions in the polymer electrolytes. Lee et al. firstly reported that boron-based compounds were effective for increasing the concentration of the carrier ions in solution electrolytes, as well as the transport number of lithium ions [23,24]. Yuki Kato et al. had studied the effect of group 13/III metal centered alkoxides, viz., $Ga(OC_2H_5)_3$, $Al(OC_2H_5)_3$ and $B(OC_2H_5)_3$, on the ionic conductivity of polymer electrolytes. Although adding $Ga(OC_2H_5)_3$ could achieve higher ionic conductivity, $B(OC_2H_5)_3$ is more suitable for being applied in Li-ion cells, considered the molecular weight of the additives and the specific energy of the cells [25]. Wakihara et al. had synthesized the tris(methoxypolyethyleneglycol)-borate ester (PEG-B), and added in the polymer electrolyte with poly(ethylene oxide) (PEO) matrix. The ionic conductivity and Li-ion transference number had been successfully increased by adding PEG-B [26,27]. And the composited polymer electrolyte exhibits good performance in the $LiMn_{1.8}Co_{0.2}O_4$ and $LiFePO_4$ cells, respectively [27,28].

Because the group 13/III elements in the plasticizers possess Lewis acidity, anions in the liquid electrolyte might be attracted to plasticizers. It is expected that these plasticizers inhibit the migration of polysulfide anions (S_n^{2-}, $3 \leq n \leq 8$) in Li–S cells, which could improve the cycle performance of Li–S cells.

In this work, we synthesized the PEG-B plasticizer, and used the composited gel polymer electrolyte (GPE) in Li–S cells. Furthermore, electrochemical impedance spectroscopies (EIS), scanning electron microscopy (SEM), X-ray Diffraction (XRD) and X-ray photoelectron spectra (XPS) were performed in order to reveal the capacity fading mechanism.

2. Experimental

2.1. Preparation of gel polymer electrolyte

The PEG-borate esters (PEG-B) were synthesized, as shown in Fig. 1, by the reaction of methoxy poly(ethylene glycol) ($CH_3O(CH_2CH_2O)_7H$, Aldrich) and boric acid anhydride (B_2O_3, Aldrich). The mixture was dissolved in toluene under N_2 atmosphere and refluxed at 110 °C to eliminate the generated water. After the completion of the reaction, toluene was evaporated under vacuum condition, and finally, clear liquid was obtained. The obtained PEG-B were preserved in Ar-filled glove box.

The matrix polymer was a copolymer of polyethylene glycol-600 dimethacrylate (PDE600, Aldrich) and polyethylene glycol-400 methacrylate (PME400, Aldrich). The polymer electrolyte films were synthesized by radical polymerization of the mixed oligomers. Appropriate amounts of PDE600, PME400, PEG-B and lithium bis-trifluoromethanesulfonimide (LiTFSI, Aldrich) were taken together in a flask, and then stirred in Ar-filled glove box. The ratio of PDE600, PME400 and PEG-B was 1:1:5. The concentration of LiTFSI was adjusted so that the molar ratio of lithium atoms to ether-oxygen atoms (EO) in the total polyethers of PDE600, PME4000 and PEG-B is 1:24 [29]. The resulting homogeneous, viscous solution was poured on a Teflon plate. By heating the solution on the plate at 80 °C for 6 h to polymerize, freestanding electrolyte films in different thicknesses were obtained, which are GPE-1: 500 μm, GPE-2: 800 μm and GPE-3: 1000 μm. To form GPE, the films were immersed in liquid electrolyte until they were swollen completely. A solution of 1.0 M LiTFSI in 1,3-dioxolane (DOL) and dimethoxyethane (DME) mixture (1:2 by weight, Novolyte Inc.) was used as liquid electrolyte.

2.2. Preparation of Li–S cells

The sulfur cathode was fabricated with sulfur, Super P carbon and PVdF binder in weight ratio of 70:20:10. The cathode slurry was prepared by ball milling and then cast onto an Al foil by using a doctor blade with typical active material loading of 2.8 mg cm^{-2}. After vacuum drying 12 h at 70 °C, the cathode was transferred into the glove box.

The Li–S cell was assembled by stacking in turn the sulfur cathode, the polymer electrolyte film, and Li foil, and then sealed with amount liquid electrolyte into CR2032 coin cell for measurements. For comparison, the standard Li–S cell with the same cathode, Li foil and liquid electrolyte, but Celgard 2400 as the separator was referred to as standard cell. The fabrication was taken in the Ar-filling glove box.

2.3. Characterization

The charge–discharge performance of the Li–S cells were evaluated by cycling the cells between 2.5 and 1.5 V at current density of 0.3 mA cm^{-2} on Land CT2001A test system (Land Corp., Wuhan, China).

The cyclic voltammogram of the Li–S cells was measured at sweep rate of 0.5 mV s^{-1}. EIS were carried out over the frequency range from 1 MHz to 0.1 Hz. Li-ion transference number (t_{Li}^{+}) of the ionomer electrolyte was determined by using the steady-state current method [30], on a coin cell assembled by sandwiching GPE between two Li foils. The method consists of initial measurement of the lithium interfacial resistance (R_0), then application of a small voltage (ΔV, 10 mV) until a steady current (I_{ss}) is obtained, and final

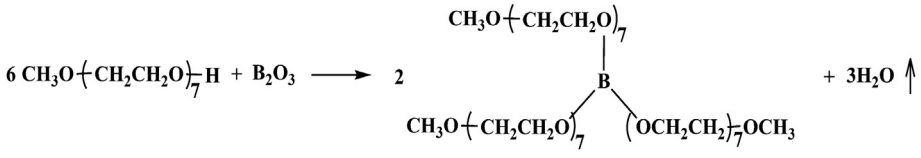

Fig. 1. Reaction for preparation of the PEG-borate from methoxy poly(ethylene glycol) and boric acid anhydride.

measurement of the interfacial resistance (R_f). Li-ion transference number (t_{Li}^{+}) is calculated using the equation $t_{Li}^{+} = I_{ss}(\Delta V - I_0R_0)/I_0(\Delta V - I_{ss}R_f)$, where I_0 is the initial current and is calculated from the voltage and the initial overall cell resistance by $I_0 = \Delta V/(R_e + R_0)$, where R_e is the electrolyte resistance. All the measurements were investigated with VersaSTAT (Princeton Applied Research).

The morphologies of the lithium anodes were investigated by scanning electron microscopy (S4800, Hitachi). XRD and XPS were applied to identify the composition of the Li anode after cycling. The XRD (Rigaku RINT-2000) were obtained using Cu Kα radiation at $\lambda = 1.54$ Å. The lithium sample was enclosed inside a polyimide bag to prevent undesirable reactions with air during XRD testing. The XPS (Thermo Fisher Scientific, K-Alpha 1063) were obtained by using Al-Kα radiation, operating at a power of 72 W (12 kV) with a base pressure of 10^{-9} Torr. The diameter of the analyzed area of the samples was 400 mm and an argon ion beam (accelerating voltage 3 keV, ion beam current 6 mA) was employed for the etching process.

3. Results and discussion

3.1. Electrochemical properties of the polymer electrolyte

The critical property is chemical and electrochemical stability of GPE over the entire potential range of anodic and cathodic reactions. Fig. 2 shows the cyclic voltammogram curve (CV) of GPE-1 sandwiched between stainless steel (SS) and Li metal electrode. In the cathodic region, it was observed that Li deposition occurred below 0 V, and Li stripping followed on the anodic sweep. The Li planting–stripping process was reversible and there was no other oxidation peaks up to 4 V. Furthermore, it is found that the current increased sharply when the potential excessed 4.5 V, which means that GPE is electrochemical stable up to 4.5 V vs. Li^+/Li.

The CV curve of Li–S cells with GPE-1 is shown in Fig. 3. The CV exhibited typical characteristic oxidation and reduction peaks of elemental sulfur. The oxidation peak at 2.50 V was attributed to the conversion of lithium polysulfide into sulfur and lithium. The two reduction peaks were corresponding to the two steps reduction of sulfur: the first at 2.35 V represents reduction of solid sulfur to soluble intermediate lithium polysulfide, and the second represents further reduction of lithium polysulfide to solid lithium sulfides [31]. No additional peaks are found in CV, indicating that the polymer electrolyte is electrochemical stability to the S cathode.

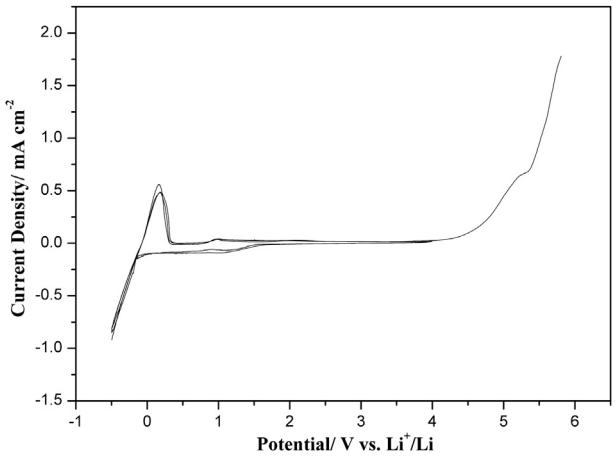

Fig. 2. Cyclic voltammogram of Li|GPE-1|SS cell from −0.5 V to 6 V at the scan rate of 0.5 mV s^{-1} at room temperature.

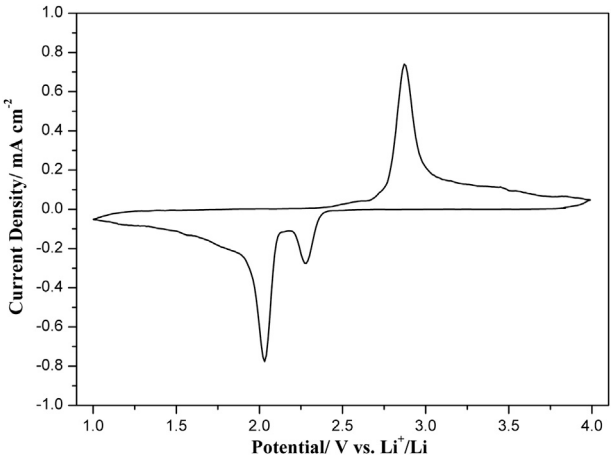

Fig. 3. Cyclic voltammogram of Li–S cell using GPE-1 from 1 V to 4 V at the scan rate of 0.5 mV s^{-1} at room temperature.

3.2. Electrochemical prosperities of the Li–S cells with GPE

The voltage profiles of the cell using GPE-1 at the initial, 5th, 10th and 20th cycles are shown in Fig. 4(a). Each discharge curve shows two voltage plateaus, corresponding to the reduction peaks in the CV curve. The discharge capacities of the cell using GPE-1, GPE-2 and GPE-3, and the standard cell are shown in Fig. 4(b),

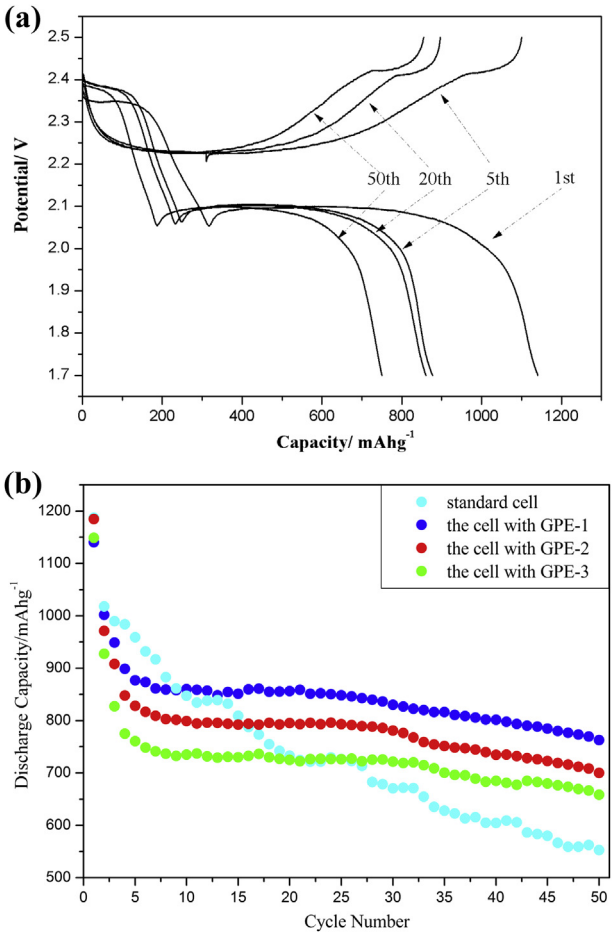

Fig. 4. Cycle performance of Li–S cell using GPE in the range of 2.5–1.5 V at current density of 0.3 mA cm^{-2} (a): the discharge/charge profile at different cycles using GPE-1. (b): The cycle performances using GPE-1, GPE-2 and GPE-3, compared with the standard cell.

respectively. The initial discharge specific capacities of the cells using the GPEs were similar to that of the standard cell. Moreover, a high irreversible discharge capacity loss (about 280 mAh g^{-1}) was found at the subsequent three cycles in both the cells using GPEs and the standard cell. However, significantly difference was observed after the 5th cycle. The discharge specific capacities of the standard cell gradual decayed with the farther cycles, while the discharge capacities of the cells using GPEs retained lasting for longer cycles, and then decayed slowly. All the cells using GPEs showed a better cycle performance than the standard cell. Among the cells with GPEs, although the variation tendency of the cells' capacities is nearly the same, there are some subtle differences. The cell using thicker GPE got longer stable cycling times but lower discharge specific capacities. For instance, the discharge specific capacity of the cell using GPE-3 began to decay at the 32nd cycle from about 720 mAh g^{-1}, while that of the cell using GPE-1 began to decay at the 25th cycle from about 850 mAh g^{-1}. The result of the cell using thicker GPE get longer stable cycling times might be combining with the gel state electrolyte and the trapping effect of PEG-B. However, compared with our other data shown in ref. [32], the gel electrolyte without the PEG-B Lewis acid additives could not achieve the same level of the stable cycle property like the GPE with PEG-B does. So it is confirmed that the PEG-B Lewis acid additives play a more important role in the cells than the gel state electrolyte does. However, the capacity retention of cells using GPE with PEG-B added doesn't reach the ideal result. The capacity fading mechanism should be clarified.

3.3. Analysis of capacity fading mechanism

The phenomenon of high discharge capacity loss in both the cells using GPEs and the standard cell at the first four cycles is not strange, which had appeared in many literatures [33–35]. This phenomenon is associated with the redox mechanism of sulfur in Li–S cells. In the CV curve of Li–S cells, typically there is only one oxidation peak. It is suggested that all the polysulfides transform into the intermediate with the most facile oxidation kinetics (via charge transfer) at the end of charge process, which is believed to be S_8^{2-} rather than $S_{8(l)}$ [36,37]. Therefore, the discharge capacity losses at the first four cycles are responding to the discharge specific capacity contributed by the electrochemical reaction: $S_{8(l)} + 2e^- = S_8^{2-}$.

The main difference between the cells using GPEs and the standard cell was the different retention rate of discharges capacities during the 5th cycle and the 30th cycle. In order to clarify the details of GPE with respect to the cycle performance, EIS of the cell using GPE-1 and the standard cell had been investigated at the end of discharge process of each cycle. Nyquist plots for the cell using GPE-1 and the standard cell (as shown in Fig. 5(a) and (b)) consist of two semicircles in a higher frequency region, and a straight line in a lower frequency region. The semicircle at high frequency is corresponding to a charge-transfer reaction at the Li anode/GPE interface, and that at low frequency side is the reaction at the GPE/S cathode interface. The straight line at lower frequency regime is a resistance attribute to the diffusion derived by concentration gradient around the GPE/S cathode interface. To perform a quantitative analysis, the impedance spectra were curve fitted by using the equivalent circuit, as shown in Fig. 6. The equivalent circuit model for Li–S cell is formed by resistance *R*, double-layer capacitance *C*, and Warburg impedance *W*. In an actual process, usually constant phase angle element (CPE) is used to replace with capacitance by taking into account the distribution of the relaxation time or the non-uniform distribution of current because of the rough nature of the electrode. Among them, R_e, R_{Li}, and R_S represent the resistance as the results of ionic conduction in the bulk of

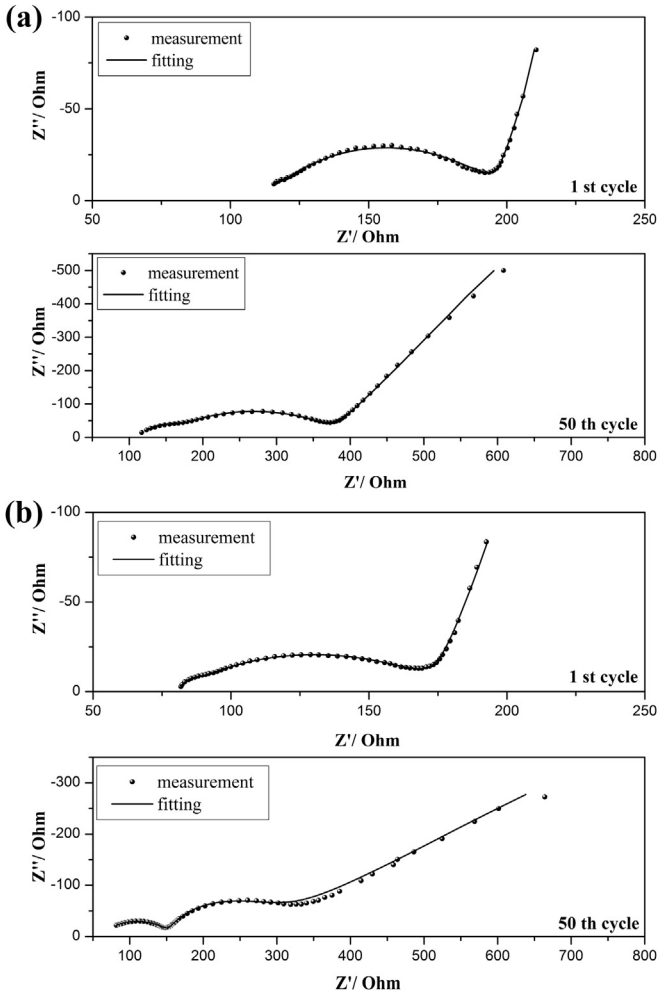

Fig. 5. Nyquist plots (symbol) for (a) the Li–S cell using GPE-1 and (b) the standard cell at 1st and 50th cycles. The fitted curves are also shown by a solid line using an equivalent circuit presented in Fig. 7.

electrolyte, charge transfer at the Li anode/electrolyte interface and at the electrolyte/S cathode interface, respectively. CPE_{Li} is a distributed capacity of the Li anode/electrolyte interface, and CPE_S is a distributed capacity of the electrolyte/S cathode interface. W_S reflects Warburg impedance as a result of the mass diffusion characteristics around the electrolyte/S cathode interface, which is parallel with a series combination of CPE_2. In the whole discharge process of the cell, Li ions are detached from the Li metal, migrate to the surface of sulfur composite cathode through electrolyte, and then react with sulfur. This is a continuous process. Therefore, electrolyte resistance, interface resistance and the charge transfer resistance are in series circuit.

Typical results of curve fitting are presented in Fig. 5, and show a good agreement of the experimental (symbol) with the calculated impedance spectra (solid line). The best results of the fitted

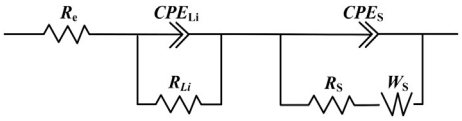

Fig. 6. Equivalent circuit for the curve fittings of EIS. R_i, CPE_i and W_i represent the resistance, capacity and Warburg impedance of component i, respectively.

resistances R_e, R_{Li} and R_S, are summarized in Fig. 7(a) and (b) as a function of cycle number for the cell using GPE-1 and the standard cell, receptivity.

In the case of the cell using GPE-1, a gradual increase of R_S was observed during all the cycles. In the stable capacity retention regime of the cell using GPE-1 during the 5th cycle and the 30th cycle, and R_e and R_{Li} remained constant. The capacity then began to decrease gradually after stable cycling up to the 30 cycles, at the meanwhile, the R_{Li} showed a discontinuous increase. A similar tendency is also observed in the case of the standard cell, in which the R_S and R_{Li} increase along with the cycles. The differences between the cell using GPE-1 and the standard cell were the numerical values of R_e and the variation tendency of R_{Li}. The initial R_e is higher for the cell using GPE-1 compared to the standard cell, given the thicker separator (500 vs. 20 μm). The stable R_{Li} was observed in the cell using GPE-1 during the 5th cycle and 25th cycle, which did not appear in the standard cell. It is suggested that the increase of resistance was indicated for R_{Li}, which corresponds to the different retention rate of discharge capacities.

The SEM, XRD and XPS were carried out to clarify the change on the Li/GPE interface. The surface morphologies of the fresh Li metal, the Li anode of the cell using GPE-1 and the standard cell after the 25th cycle, and after the 50th cycle are shown in Fig. 8(a)–(e), respectively. It is observed that precipitations were found on the Li anode surface of the standard cell and the cell with GPE after 50th cycle, while not any precipitations were found by eyes on the surface of the fresh Li metal and the Li anode of the cell using GPE-1 after 25th cycle. For more detail, XRD and XPS of the Li anode of the cell using GPE-1 are carried out to determine chemical composition of the precipitations. The XRD spectra are shown in Fig. 9. As indicated in Fig. 9(a), the polyimide film displayed no any sharp diffraction peaks besides a broad band at the lower diffraction angle. Fig. 9(b) shows the XRD pattern of the fresh Li metal, indicating two crystal peaks indexed to the Li metal. Li_2S phase was observed from the lithium anode of the cell with GPE after 50th cycle, while no Li_2S phase was observed from the lithium anode of the cell with GPE after 25th cycle, as shown in Fig. 9(c) and (d). No B_{1s} signal was found on the surface of the Li anodes of the cells using GPE-1 after 25th cycle and 50th cycle in XPS measurement, which means that PEG-B didn't affect the interface stability of GPE/Li anode. The XPS S_{2p} spectra of the Li anodes of the cells using GPE-1 after 25th cycle and 50th cycle are shown in Fig. 10. The peak at 160.0 eV was assigned to Li_2S, the peak at 161.1 eV was assigned to Li_2S_2, the peak at 163.5 eV was assigned to $Li_2S_2O_3$, the peak at 166.9 eV was assigned to Li_2SO_3, and the peak at 169.0 eV was assigned to $-NSO_2CF_3$. The $Li_2S_2O_3$, Li_2SO_3, $-NSO_2CF_3$ and part of Li_2S and Li_2S_2 were attributed to products of LiTFSI decomposition on Li anode [12], and other part of Li_2S and Li_2S_2 were attributed to the reaction of soluble polysulfide and Li. As shown in Fig. 10, the S signal was disappeared after etching 180 s on the surface of Li anode after 25th cycle, while this signal was still detected after etching 720 s on the surface of Li anode after 25th cycle, which means that both the thickness of solid electrolyte interphase (SEI) and the content of Li_2S produced by soluble polysulfide in the SEI on the surface of Li anode after 25th cycle were less than those on the surface of Li anode after 50th cycle.

Combined with SEM, XRD and XPS, it could be concluded that the precipitations on the Li surface are mainly made of Li_2S, which are highly insulative, and would not take part in electrochemical oxidation during the next charge processes when they has precipitated on the surface of Li anode. However, less Li_2S corrosion products were found on the Li anode after 25 cycles in the cell using GPE-1. It is suggested that Li_2S corresponds to the increase of R_{Li}.

The formation of Li_2S was controlled by the ionic transmission in electrolyte. The ionic conductivity and t_{Li}^{+} of GPE-1 before cycling, after the 25th cycles, and after the 50th cycle in Li–S cells are

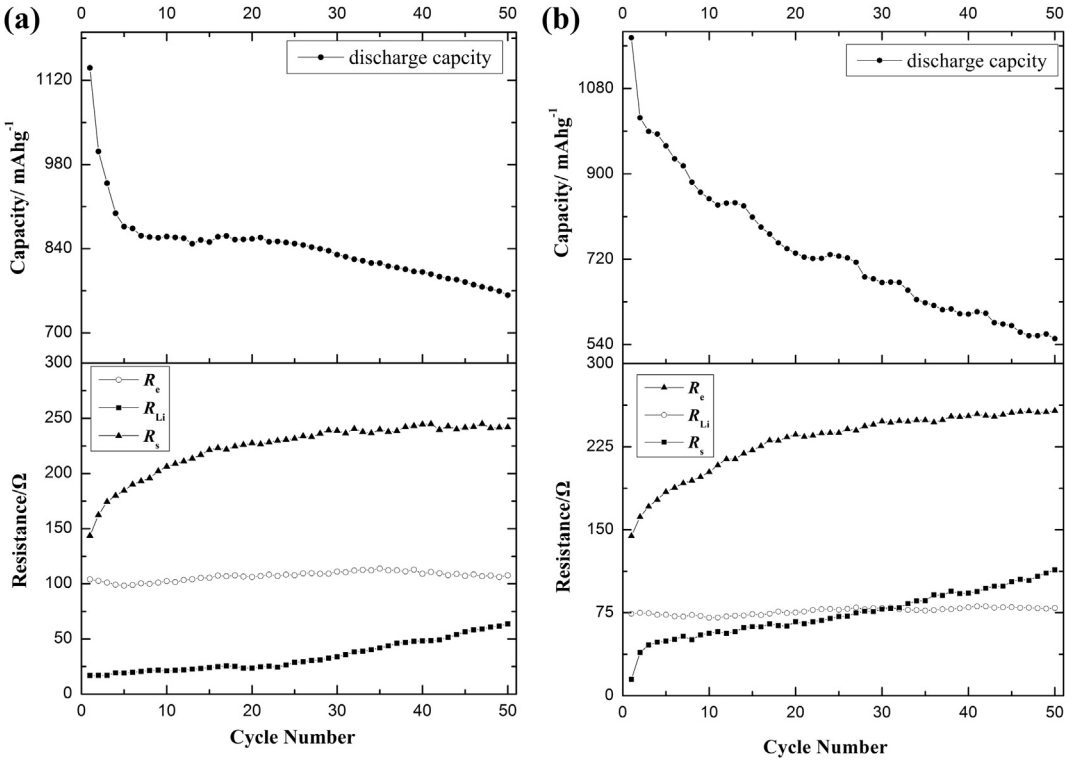

Fig. 7. Variation of each resistance verse cycle number of (a) the Li–S cell using GPE-1 and (b) the standard cell. R_e, R_{Li} and R_S correspond to the resistances due to bulk of electrolyte, Li| electrolyte interface and electrolyte| cathode interface, respectively.

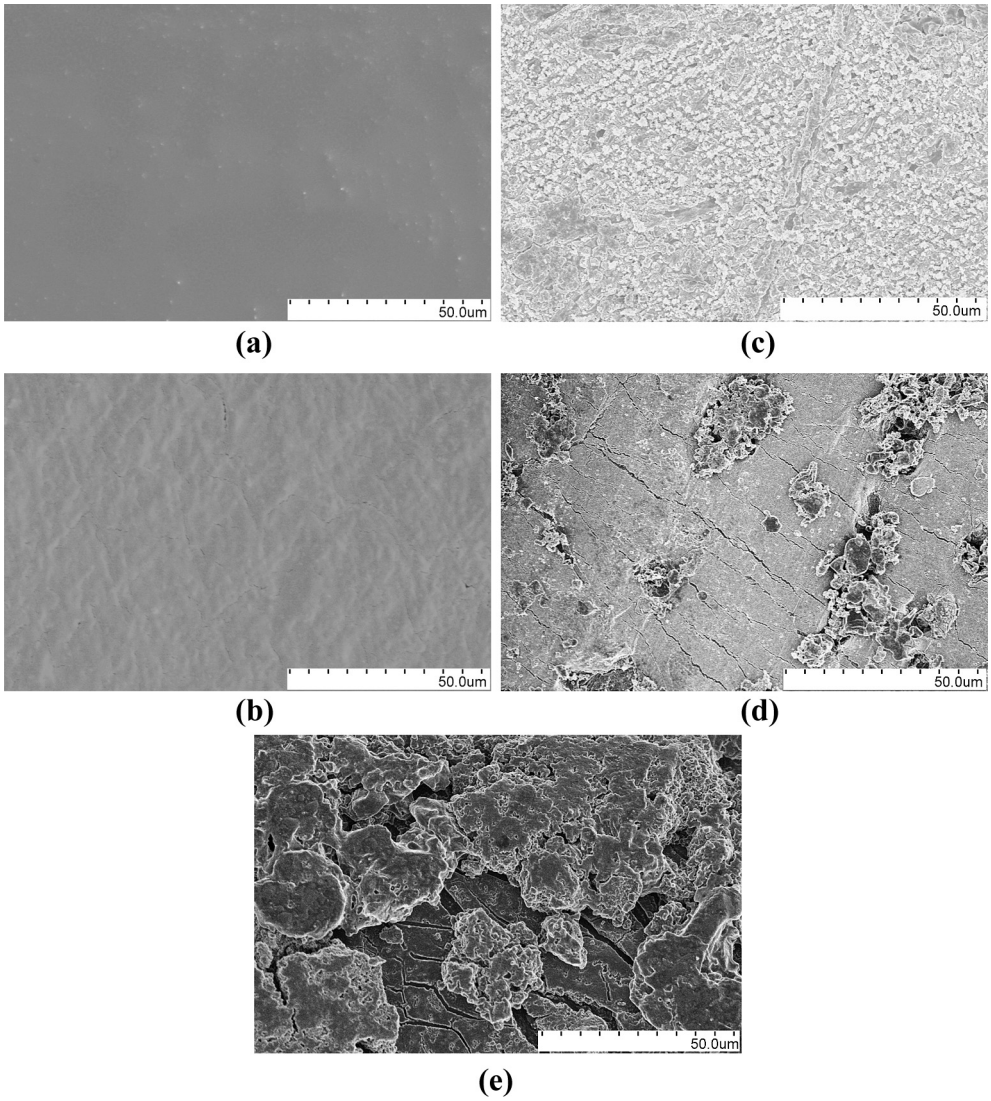

Fig. 8. SEM of (a) fresh Li; (b) Li anode cycled in the Li–S cell with GPE-1 after 25th discharged; (c) Li anode cycled in the Li–S cell with GPE-1 after 50th discharged; (d) Li anode cycled in the standard cell after 25th discharged; (e) Li anode cycled in the standard cell after 50th discharged.

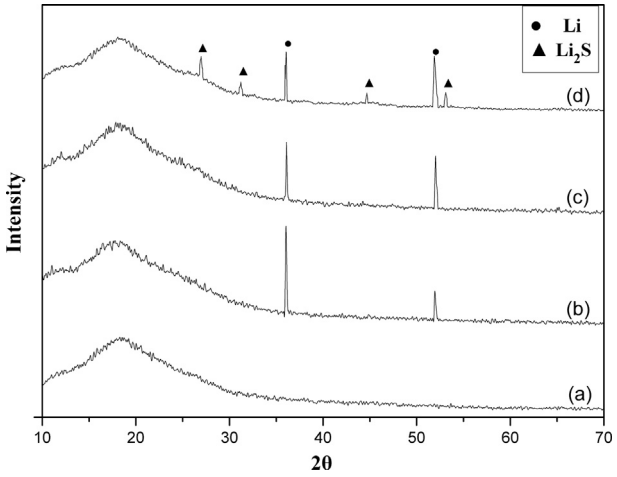

Fig. 9. XRD patterns of (a) polyimide film; (b) fresh Li; (c) Li anode cycled in the Li–S with GPE-1 after 25th discharged; (d) Li anode cycled in the Li–S with GPE-1 after 50th discharged.

presented in Table 1. For the comparison, the ionic conductivity and t_{Li}^{+} of Celgard 2400 with liquid electrolyte are also included. The ionic conductivity of both GPE-1 and liquid electrolyte increased in some extent after cycled in the Li–S cells, which is caused by the increase of concentration of Li salt in electrolyte, for the intermediate lithium polysulfide dissolve in electrolyte. The t_{Li}^{+} of GPE-1 was higher than that of liquid electrolyte, and still increase after cycled in Li–S cells, which was attributed to the existing of PEG-B. PEG-B ester is known as Lewis acid, which could interact with anion [38,39]. Polysulfide anions dissolve in GPE and then are trapped by PEG-B, resulting in a stable cycle property during the later cycles, for the trapped polysulfide anions in GPE couldn't transport through the electrolyte. If the polysulfide anions could not react with metal Li, Li_2S would not form on Li anode surface, and finally, Li–S cells with stable cycle property were obtained. Unfortunately, t_{Li}^{+} of GPE-1 decreased after 50th cycle, which means that the PEG-B couldn't trap polysulfide anions permanently. The possible reason is that polysulfide anions would diffuse toward Li anode by the void space between each B atom, limited by the areal density of B atom in GPE.

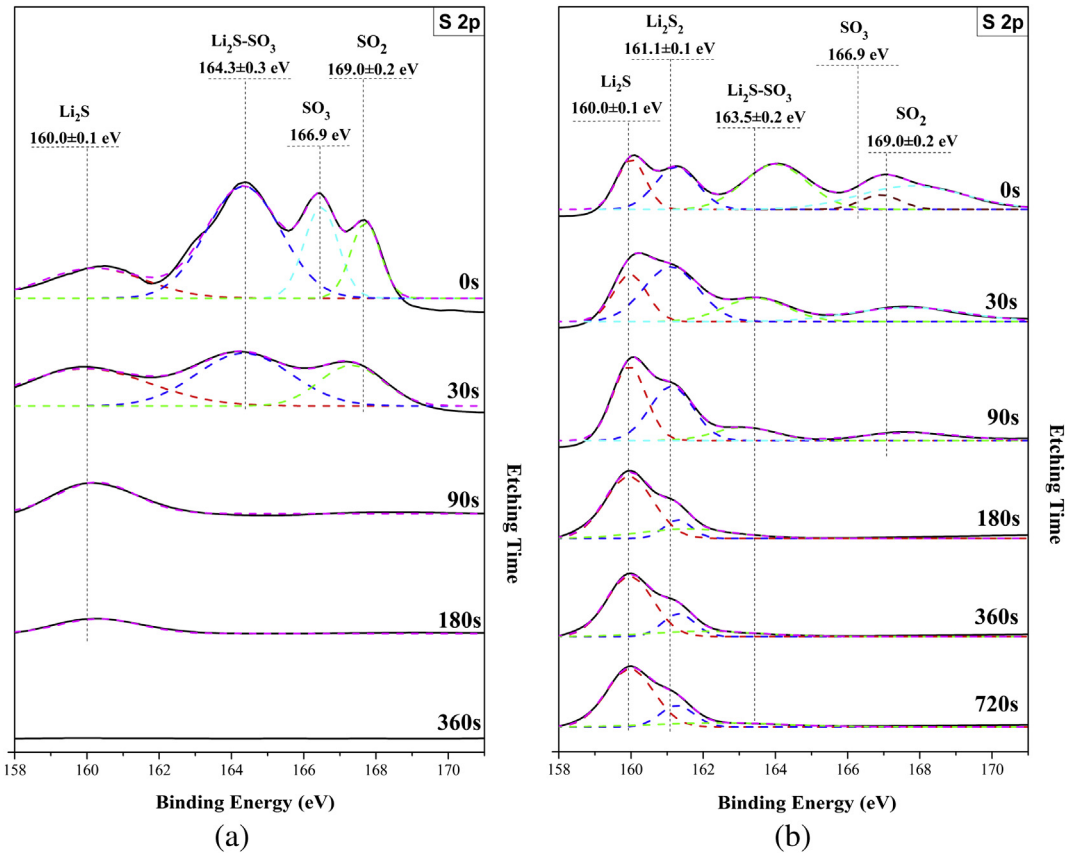

Fig. 10. XPS S_{2p} spectra of the Li anodes of the cells using GPE-1 (a) after 25th cycle and (b) after 50th cycle.

Table 1
The ionic conductivity and Li-ion transference number of initial GPE-1, GPE-1 after 20 cycles, GPE-1 after 50 cycles and the Celgard in liquid electrolyte.

Electrolyte	$\sigma/10^{-4}$, S cm^{-1}	t_{Li}^{+}
GPE-1 initial	3.34 ± 0.11	0.54 ± 0.01
GPE-1 after 20 cycles	3.73 ± 0.12	0.86 ± 0.02
GPE-1 after 50 cycles	3.6 ± 0.11	0.73 ± 0.01
Celgard in liquid electrolyte	7.6 ± 0.15	0.29 ± 0.01

σ: ionic conductivity, t_{Li}^{+}: Li-ion transference number.

4. Conclusion

Using EIS, SEM, XRD and XPS, we analyzed the capacity fading mechanism in the Li–S cells using GPE that contains PEG-B ester. The decrease of capacities is related to an undesirable side reaction that occurs at the GPE/Li anode interface, caused by the diffusion of polysulfide anions. PEG-B ester could not trap the polysulfide anions completely. Accordingly, using a functional electrolyte, which could prevent polysulfide anions transporting through completely, would improve the cycle performance of Li–S cells in an even better fashion.

Acknowledgements

Aid program for Science and Technology Innovative Research Team in Higher Education Institutions for Hunan Province.

References

[1] K. Kumaresan, Y. Mikhaylik, R.E. White, J. Electrochem. Soc. 155 (2008) A576.
[2] V.S. Kolosnitsyn, E.V. Karaseva, Russ. J. Electrochem. 44 (2008) 506.
[3] E. Peled, Y. Sternberg, J. Electrochem. Soc. 136 (1989) 2.
[4] D. Marmorstein, T. Yu, K. Striebel, J. Power Sources 89 (2000) 219.
[5] B. Jeon, J. Yeon, K. Kim, I. Chung, J. Power Sources 109 (2002) 89.
[6] J. Akridge, Solid State Ionics 175 (2004) 243.
[7] H. Ryu, Z. Guo, H. Ahn, G. Cho, H. Liu, J. Power Sources 189 (2009) 1179.
[8] C. Barchasz, J.-C. Leprêtre, F. Alloin, S. Patoux, J. Power Sources 199 (2012) 322.
[9] X. Ji, K.T.K. Lee, L.L.F. Nazar, Nat. Mater. 8 (2009) 500.
[10] F. Wu, J. Chen, L. Li, T. Zhao, R. Chen, J. Phys. Chem. C 115 (2011) 24411.
[11] Y. Cao, X. Li, I.A. Aksay, J. Lemmon, Z. Nie, Z. Yang, Phys. Chem. Chem. Phys. 13 (2011) 7660.
[12] D. Aurbach, E. Pollak, R. Elazari, G. Salitra, C.S. Kelley, J. Affinito, J. Electrochem. Soc. 156 (2009) 694.
[13] X. Liang, Z. Wen, Y. Liu, M. Wu, J. Jin, H. Zhang, X. Wu, J. Power Sources 196 (2011) 9839.
[14] S.S. Zhang, Electrochim. Acta 70 (2012) 344.
[15] J. Choi, G. Cheruvally, D. Kim, J. Ahn, K. Kim, H. Ahn, J. Power Sources 183 (2008) 441.
[16] F. Lin, J. Wang, H. Jia, C.W. Monroe, J. Yang, Y. Nuli, J. Power Sources 223 (2013) 18.
[17] Z. Lin, Z. Liu, W. Fu, N.J. Dudney, C. Liang, Adv. Funct. Mater. 23 (2013) 1064.
[18] Z. Jin, K. Xie, X. Hong, Z. Hu, X. Liu, J. Power Sources 218 (2012) 163.
[19] L.X. Yuan, J.K. Feng, X.P. Ai, Y.L. Cao, S.L. Chen, H.X. Yang, Electrochem. Commun. 8 (2006) 610.
[20] J. Jin, Z. Wen, X. Liang, Y. Cui, X. Wu, Solid State Ionics 225 (2012) 604.
[21] M. Nagao, Y. Imade, H. Narisawa, T. Kobayashi, R. Watanabe, T. Yokoi, T. Tatsumi, R. Kanno, J. Power Sources 222 (2013) 237.
[22] T. Kobayashi, Y. Imade, D. Shishihara, K. Homma, M. Nagao, R. Watanabe, T. Yokoi, A. Yamada, R. Kanno, T. Tatsumi, J. Power Sources 182 (2008) 621.
[23] H.S. Lee, X.Q. Yang, J. McBreen, L.S. Choi, Y. Okamoto, J. Electrochem. Soc. 143 (1996) 3825.
[24] H.S. Lee, X.Q. Yang, C.L. Xiang, J. McBreen, J. Electrochem. Soc. 145 (1998) 2813.
[25] Y. Kato, K. Hasumi, Y. Uchimoto, Solid State Ionics 172 (2004) 63.
[26] Y. Masuda, M. Seki, M. Nakayama, M. Wakihara, H. Mita, Solid State Ionics 177 (2006) 843.
[27] I.R.M. Kottegoda, Z. Bakenov, H. Ikuta, M. Wakihara, J. Electrochem. Soc. 152 (2005) A1533.
[28] F. Kaneko, S. Wada, M. Nakayama, M. Wakihara, J. Koki, S. Kuroki, Adv. Funct. Mater. 19 (2009) 918.
[29] Y. Kato, K. Hasumi, S. Yokoyama, T. Yabe, H. Ikuta, Solid State Ionics 150 (2002) 355.

[30] P.G. Bruce, C.A. Vincent, J. Electroanal. Chem. 1 (1987) 225.
[31] Y. Mikhaylik, J. Akridge, J. Electrochem. Soc. 151 (2004) A1969.
[32] Z. Jin, K. Xie, X. Hong, RSC Adv. (2013), http://dx.doi.org/10.1039/c3ra41517a.
[33] Y. Yang, G. Yu, J.J. Cha, H. Wu, M. Vosgueritchian, Y. Yao, Z. Bao, Y. Cui, ACS Nano 5 (2011) 9187.
[34] H. Sun, G.-L. Xu, Y.-F. Xu, S.-G. Sun, X. Zhang, Y. Qiu, S. Yang, Nano Res. 5 (2012) 726.
[35] W. Ahn, K.-B. Kim, K.-N. Jung, K.-H. Shin, C.-S. Jin, J. Power Sources 202 (2012) 394.
[36] X. Ji, L.F. Nazar, J. Mater. Chem. 20 (2010) 9821.
[37] Y. Jung, S. Kim, B. Kim, D. Han, S. Park, J. Kwak, Int. J. Electrochem. Sci. 3 (2008) 566.
[38] Y. Kato, K. Suwa, H. Ikuta, Y. Uchimoto, J. Mater. Chem. 13 (2003) 280.
[39] Y. Kato, K. Hasumi, Y. Uchimoto, M. Wakihara, Solid State Ionics 172 (2004) 63.